In situ stabilized carbon nanofiber (CNF) reinforced epoxy nanocomposites†

Jiahua Zhu,[a] Suying Wei,*[b] Jongeun Ryu,[c] Mahesh Budhathoki,[a] Gang Liang[d] and Zhanhu Guo*[a]

Received 18th January 2010, Accepted 18th March 2010
First published as an Advance Article on the web 10th May 2010
DOI: 10.1039/c0jm00063a

Carbon nanofibers (CNFs) suspended epoxy resin nanocomposites and the corresponding polymer nanocomposites are fabricated. The surface of CNFs is introduced a functional amine terminated groups *via* silanization, which in situ react with epoxy monomers. This in situ reaction favors the CNFs dispersion and improves the interfacial interaction between CNFs and monomers. Effects of particle loading, surface treatment and operating temperatures of rheological tests on the complex viscosity, storage modulus and loss modulus are systematically studied. Unique rheological phenomena "a decreased viscosity with a better dispersion" are observed and explained in terms of the improved filler dispersion quality. Meanwhile, significant increase in the tensile property and storage modulus is observed and related to the better dispersion and the introduced strong interfacial interaction as revealed by SEM imaging. Finally, electrical conductivity is investigated and an unusual deficiency of surface treatment to improve the electrical conductivity is explained by an insulating coating layer.

1. Introduction

Incorporation of inorganic fillers, such as fibers, particles with micrometric or nanometric dimensions, into polymeric materials has been a common way to fabricate high-performance materials in modern industries.[1–7] Polymer nanocomposites (PNCs) concentrate on the fabrication of advanced materials, which combine the advantages of both polymer and nanomaterials. Such materials have attracted considerable attention in both academic and industrial fields in recent years for their diverse potential applications such as energy storage devices,[8,9] electronics,[10–12] sensors,[13–16] and bio-applications.[17,18]

Epoxy represents one of the most important engineering polymers and has found wide applications such as adhesives[19] and electronics encapsulation materials.[20] It has also replaced steels as structural parts in airplanes and satellites owing to its high mechanical strength.[21] In most of the applications, for example additives, carbon fibers, graphites, carbon blacks and carbon nanotubes (CNTs) are often used to improve the mechanical properties and electrical conductivity.[22–24] Other composites containing silicate[25] or clays[26,27] have attracted tremendous interest due to the improved thermal stability, which is essential in fire retardant materials. However, the properties of inorganic–organic composites greatly depend on the interfacial interaction between the reinforcing materials and the polymer matrices.[28–30] In other words, all the high-quality PNCs will definitely have to solve two common challenges: (1) uniform dispersion of the nanomaterials in a polymer matrix, and (2) interfacial compatibility of the nanofillers with the polymer matrix. These challenges are much more obviously encountered in carbon based nanomaterials, such as carbon nanofibers (CNFs) and CNTs, which show inert characteristics because of the graphite structure on the surface.[31] As a result, various methods have been conducted to tailor the surface properties of CNFs and CNTs.[32]

Among the various methods which had been studied until now, chemical approach is positioned in the most active area due to its easy design of the surface properties and other physico-chemical properties.[32–38] Wong *et al.* reported covalent chemical strategies for the functionalization of CNTs from the structural perspective, and proposed that the reaction on CNTs can proceed not only at the tube ends and defect sites but also along the side walls. Ultimately, the electronic and mechanical properties can be tailored in a determinable manner.[34] Various other methods of chemical modification on CNTs are summarized by Tasis *et al.*[32] Though CNTs have been widely studied, CNFs possess lower manufacturing costs relative to CNTs while maintaining large aspect ratio and high mechanical and electrical properties, which make CNFs promising candidates for the development of novel PNCs in large quantities.

The rheological property is essentially important for the processing of PNCs. Meanwhile, it provides a convenient way to evaluate the dispersion state of the nanofillers in the polymer matrix.[39,40] The shear response of the PNCs is one of the most important characteristics of the rheological properties, which provides essential parameters of the PNCs processability. The dispersion of the nanofillers in the epoxy resin is hard to control during the curing process because of the increased viscosity as the polymerization proceeds between the monomers and the curing agent. Therefore, researchers turn to study the dispersion of the nanofillers in the precursor instead of the sample after curing for

[a]*Integrated Composites Laboratory (ICL), Dan F Smith Department of Chemical Engineering, Lamar University, Beaumont, TX, 77710, USA. E-mail: zhanhu.guo@lamar.edu; Tel: (+409) 880-7654*
[b]*Department of Chemistry and Physics, Lamar University, Beaumont, TX, 77710, USA. E-mail: suying.wei@lamar.edu*
[c]*Department of Mechanical & Aerospace Engineering, University of California Los Angeles, Los Angeles, CA, 90095, USA*
[d]*Materials Characterization Facility Center, Texas A&M University, College Station, TX, 77843, USA*
† Electronic supplementary information (ESI) available: DSC curves of the pure epoxy and CNF/epoxy nanocomposites. See DOI: 10.1039/c0jm00063a

such materials.[41,42] However, relatively few works have been reported until now.

In the previous studies, the dispersion and interfacial compatibility of CNFs are either separately investigated or are achieved by more complicated steps. However, the enhancements of both dispersion and interfacial interaction through one step are in great demand. To the best of our knowledge, there have been few preceding reports on CNF dispersion in an epoxy matrix *via* covalent bonding to enhance the dispersion and interfacial interaction simultaneously through a one step facile in situ reaction. In the present work, a bifunctional silane agent, 3-aminopropyltriethoxysilane (APTES), is used to engineering the CNFs (s-CNFs), which are then processed into epoxy resin nanocomposites. The PNCs filled with as-received CNFs (u-CNFs) are also obtained for comparison. The rheological, mechanical and thermal properties of the two types of PNCs are comparatively investigated and detailed in the following.

2. Experimental

2.1 Materials

The epoxies used are Epon 862 (bisphenol F epoxy) and EpiCure curing agent W, which are purchased from Miller-Stephenson Chemical Company, Inc. 3-Aminopropyltriethoxysilane (APTES) coupling agent with purity of 99% is purchased from Aldrich. The molecular structures of these chemicals are shown in Fig. 1. Vapor grown carbon nanofibers (CNFs, grade PR-24-XT-LHT) with an average diameter of 150 nm and a length of 50–200 μm are obtained from Pyrograf Products, Inc. According to the data from the manufacturer, the CNFs are produced by a chemical vapor deposition (CVD) process and further heated to 1500 °C to convert deposited amorphous carbon present on the surface of the fiber to a short range ordered structure. Concentrated nitric acid (HNO_3) and ethanol are provided by Fisher Scientific.

2.2 Oxidation and silanization of carbon nanofibers

Oxidation. Carbon nanofibers are oxidized in a concentrated nitric acid *via* mechanical stirring at room temperature for half an hour. Deionized (DI) water is used to wash the filtrate until it has a pH value of approximately 7. Then the CNFs obtained are dried in a vacuum oven at 80 °C overnight.

Silanization. The oxidized CNFs are added to toluene and ultrasonically stirred for one hour. APTES (1 wt% of CNFs) is subsequently added into the mixture and then refluxed at 110 °C for 8 h. The silanized CNFs are then filtered and washed several times with DI water, ethanol and acetone in sequence. The final product is dried in a vacuum oven at 80 °C overnight.

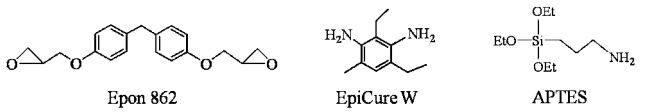

Fig. 1 Molecular structure of chemicals used in this work.

2.3 Preparation of CNF/epoxy nanocomposites

2.3.1 CNF/epoxy resin nanocomposite suspension. Epoxy resin solutions suspended with 0.1, 0.3, 0.5, 1.0 and 2.0 wt% of CNFs are prepared. Both the as-received and chemically treated CNFs are dispersed into the epoxy resin monomers, which are allowed to completely wet the CNFs overnight without any disturbance. Then the wet solution is mechanically stirred for one hour (600 rpm, Heidolph, RZR 2041) followed by sonication for one additional hour. All operations are carried out at room temperature.

2.3.2 Cured CNF/epoxy nanocomposites. The curing agent W is added to pure epoxy monomers or the above prepared CNF suspended resin solutions with a monomer/curing agent weight ratio of 100/26.5, as recommended by the Miller-Stephenson Chemical Company. High-speed (600 rpm) mechanical stirring is conducted for one hour at room temperature followed by sonication at 60 °C for one additional hour to disperse the CNFs. Then, low-speed (200 rpm) mechanical stirring is performed at 70 °C for 3–4 h in a water bath, which is essential to remove the bubbles in the solution and also to prevent the settlement of CNFs during the curing process. Finally, the solutions are poured into silicon molds and cured at 120 °C for 5 h and then cooled to room temperature naturally. Chart 1 shows the scheme of formation of s-CNF/epoxy nanocomposites.

2.4 Characterization

Rheological characterization of liquid epoxy suspensions. Dynamic rheological measurements are performed in an AR 2000ex Rheometer from TA Instrumental Company (ETC system). A series of measurements are performed in a cone-plate geometry with a diameter of 40 mm and a truncation of 64 μm. The measurements are done at 25, 50C, 75 and 120 °C, respectively. Frequency sweeping between 0.1 and 1000 1/s is carried out at a low strain (1%), which is justified to be within the linear viscoelastic (LVE) range for these materials. The LVE range is determined by the strain-storage modulus (G′) curve within the strain range from 0.01% to 100% at a frequency of 1 rad/s. Specimens placed between the cone and plate are allowed to equilibrate for approximately two minutes prior to each frequency sweeping.

Mechanical characterization of cured epoxy nanocomposites. Dynamic mechanical analyses are carried out in the torsion rectangular mode using an AR 2000ex (TA Instrumental Company) with a strain of 0.05%, a frequency of 1 Hz and a heating rate of 2 °C/min in the range of 30–200 °C. The sample dimensions are 12 × 3 × 40 mm^3. Tensile tests are carried out following the American Society for Testing and Materials (ASTM, 2002, standard D 412-98a) standard in a unidirectional tensile testing machine (COMTEN Industries, Model No. 945KRC0300; Loading unit, PSB5000). The parameters (displacement and force) are controlled by a digital controller (COMTEM, DMC 026S) with C-TAP 3.0 software from National Instruments with the Lab Windows working station. The samples are prepared as described for PNC fabrication in molds, which are designed according to the standard ASTM

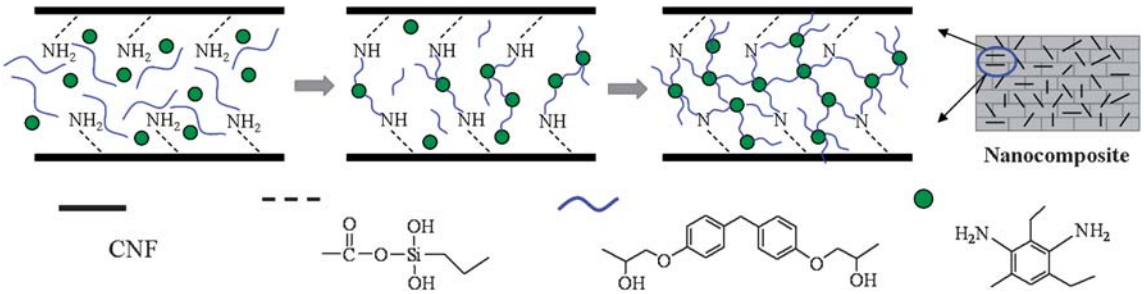

Chart 1 Schematic illustration of the in situ reinforcement of functionalized CNFs in an epoxy matrix, the bottom symbols represent the chemical structures.

requirement. A crosshead speed of 1.52 mm/min is used and the strain (mm/mm) is calculated by dividing the crosshead displacement by the original gage length.

Morphological characterization of cured epoxy nanocomposites. The dispersion quality of the CNFs with and without surface treatment in epoxy resin is monitored by microscopes Olympus SZX 7 and Leitz wetzlar for higher magnification. The morphology of the fracture surface is characterized with a scanning electron microscope (SEM, JEOL field emission scanning electron microscope, JSM-6700F). The SEM specimens are prepared by sputter coating a thin gold layer approximately 3 nm thick.

Curing extent of epoxy nanocomposites. The particle loading and functionalization effect on the curing is investigated by differential scanning calorimetry (DSC, Perkin Elmer Instruments) under 10 cm^3/min nitrogen flow conditions. The testing temperature is from 25 to 300 °C with a heating rate of 20 °C/min. The reaction enthalpy (J/g) and residual heat of the reaction are measured from the area under the DSC peaks.

Thermal characterization of cured epoxy nanocomposites. The thermal stability of the cured epoxy nanocomposites with different CNFs loadings is studied with thermogravimetric analysis (TGA, TA instruments TGA Q-500). TGA is conducted on the cured pure epoxy and u-CNF/epoxy and s-CNF/epoxy nanocomposites from 25 °C to 800 °C with a nitrogen flow rate of 60 ml/min and a heating rate of 10 °C/min.

Electrical conductivity measurement. The volume resistivity is determined by measuring the DC resistance along the length direction of rectangular bars (approximately 40 mm). An Agilent 4339B high resistance meter is used to measure the samples. This equipment allows resistivity measurement up to 10^{16} Ω. The source voltage is adjusted according to the resistivity and it is 100 V for pristine epoxy and nanocomposites with s-CNFs. However, it is set to 10 V for nanocomposites with loadings up to 0.3 wt% u-CNFs and 0.1 V for nanocomposites with loadings of 0.5 wt% and even higher CNFs. The resistivity is then converted to volume resistivity, ρ_v, using the following equation

$$\rho_v = WDR_v/L \quad (1)$$

where W is the width, D is the thickness, L is the length of the sample, and R_v is the measured resistance. The reported values represent the mean value of eight measurements with a deviation less than 10%.

3. Results and discussion

3.1 Surface treatment of CNFs and the curing process

To improve the interfacial interaction between CNFs and epoxy matrix, CNFs are firstly oxidized with nitric acid and then functionalized with APTES to introduce active amine groups on the CNF surface. The microstructure of the as-received and surface treated CNFs are shown in Fig. 2. Fig. 2(a) shows the smooth surface of the as-received CNFs. After oxidation with nitric acid, the surface becomes relatively rough, which is attributed to the etching of CNFs by strong acid, Fig. 2(b). After

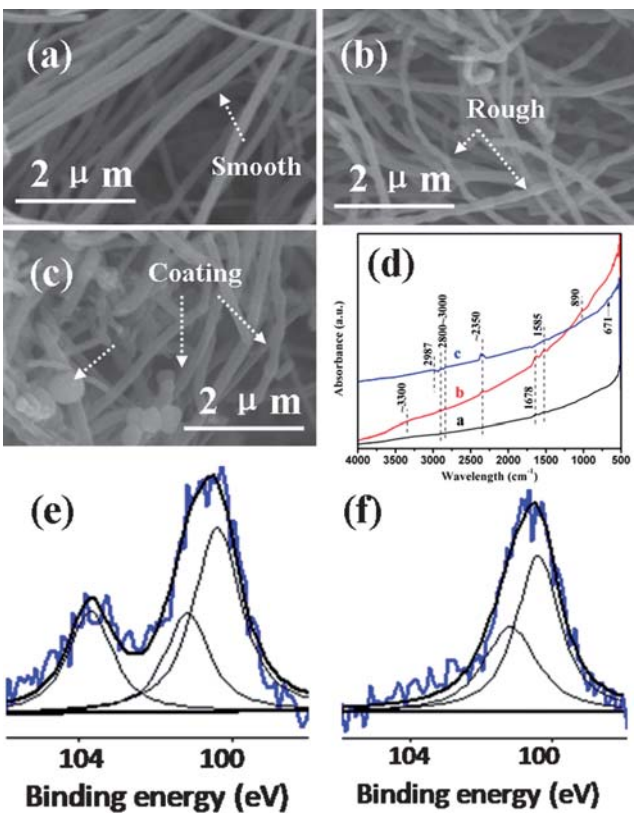

Fig. 2 SEM microstructures of (a) as-received, (b) oxidized, (c) silanized CNFs, (d) FT-IR spectra of the corresponding CNFs, and high resolution Si2p XPS spectra of (e) silanized and (f) as-received CNFs.

silanization, CNFs seem to be wrapped with a thin layer and some small pallet-like particles are observed, which are formed from the hydrolyzed APTES, Fig. 2(c). Surface modification successfully changes the surface properties of CNFs while the fiber dimensions remain unchanged.

The surface functional groups are verified by FTIR-ATR analysis. All three spectra exhibit the C–H stretching bands in the region of 3000–2800 cm^{-1} and the double CO_2 bands around 2350 cm^{-1}, Fig. 2(d). Due to the hydrogen bonding, carboxylic acid groups (–COOH) in the solid phase exhibit a broad band at ~3300 cm^{-1} corresponding to O–H stretching. This obvious characteristic band in the oxidized CNFs confirms the successful oxidation of the CNFs. The carboxylic acid C=O stretching band at 1678 cm^{-1} and the broad carboxylic acid OH deformation band at around 890 cm^{-1} further verify the successful carboxylation process. In the silanized CNFs, the band at 1585 cm^{-1} arises from the primary amine of APTES introduced during silanization.[43] An additional CH band at around 2987 cm^{-1} and weak N–H bending bonds[44] at 671 cm^{-1}, observed in the silanized rather than in the as-received and oxidized fibers, indicate that APTES has been successfully covalently linked to fibers.

APTES with bi-functional groups of hydrolysable groups ($–Si(OCH_3)_3$) and amine groups has been used as a coupling agent for the functionalization of different nanomaterials such as TiO_2,[45,46] Fe_3O_4,[47] and CNTs[48] to introduce amine functional groups. The first functional group can be hydrolyzed and chemically bound to the oxidized fiber surface while the latter can serve as catalyst and be copolymerized with the resin to form a nanocomposite. XPS is further used to characterize the silanization of CNTs. Fig. 2(e, f) show XPS data to confirm the success of silanization on the s-CNF sample. Elemental silicon is observed in the XPS spectrum, and deconvolution is done on the high-resolution Si2p spectra of both u-CNF and s-CNF with the *xpspeak41* program. A new peak is observed in the s-CNF spectrum around 103.7 eV, which is attributed to the formed network of O=C–O–Si–R on the s-CNF surface due to the silanization with APTES. This is a similar network to the Si–O–Si–R as reported on the APTES modified silica surfaces. It appears at relatively higher binding energy (103.7 eV compared to 102.4 eV),[49] because the electron-withdrawing carbonyl group reduced the electron density on the Si atom. In summary, the curing processes of pure epoxy resin and the surface treated CNFs with epoxy monomers are presented in Chart 2. Each amine group in EpiCure W will react with two epoxy monomers, which means that the two components will cross-link to form a network structure. For the s-CNFs, the CNFs surface is functionalized with amine groups after oxidation and silanization, which react with epoxy monomers. Finally, the CNFs are strongly linked with the epoxy matrix through covalent bonds.

3.2 Rheological behavior

3.2.1 Effect of CNFs loading. Fig. 3 shows the viscosity as a function the filler loading in the CNF suspended epoxy resin nanocomposite solutions. The viscosity increases with the increase of the CNFs loading and decreases with the increase of shear rate, Fig. 3(a). As expected, Newtonian behavior (viscosity is independent of shear rate) is observed for the pure epoxy resin with shear rate lower than 400 1/s and decreased viscosity is observed at the shear rate larger than 400 1/s, which is due to the increased temperature arising from the viscous heating phenomenon.[50–52] Compared to that of the pristine epoxy resin, the viscosity of the u-CNFs/epoxy solutions increases slightly as the filler loading increases to 0.5 wt%, and similar Newtonian behavior at low shear rate (<500 1/s) and shear thinning phenomenon (viscosity decreases with the increase of shear rate) are observed at high shear rate (>500 1/s). As the loading of u-CNFs further increases to 1 wt% and 2 wt%, the viscosity increases significantly, which is about 7 (1 wt%) and 50 (2 wt%) times larger than that of the pristine epoxy resin and the lower-loaded nanocomposites at the shear rate of 0.3 1/s. Furthermore, strong shear thinning is observed for the nanocomposites filled with 1 wt% and 2 wt% u-CNFs, the viscosity decreases linearly with an increase of the shear rates. This observation is significantly different from the nanocomposites filled with nanoclays, where the viscosity curves possess two distinctive regions:

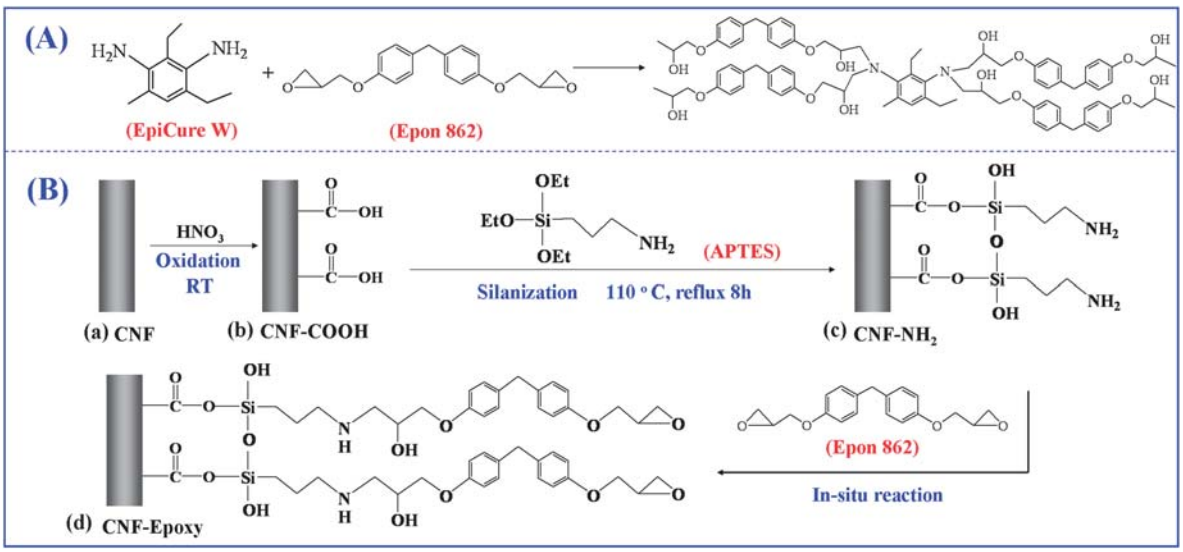

Chart 2 Curing mechanisms of (A) pure epoxy and (B) s-CNFs with epoxy monomer.

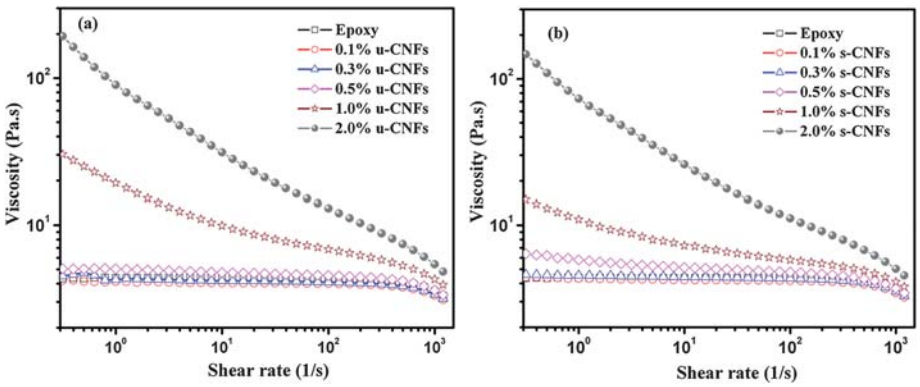

Fig. 3 Viscosity *vs.* shear rate of epoxy nanocomposites filled with different loadings of (a) u-CNFs and (b) s-CNFs at 25 °C.

a Newtonian region followed by a shear-thinning region.[53,54] The Newtonian region is caused by the confinement effect of the two-dimensional nanolayers on the polymer molecular chains, which increase the resistance to external stresses, while the shear thinning is a result of the orientation of the nanoclays parallel to the flow direction.[53,54]

The increased viscosity is mainly induced by the formed network structure of CNFs within the polymer matrix. Similar viscosity as the pristine epoxy is observed before the network is formed at low filler loadings, and the viscosity increases significantly once the network is formed at higher fiber loadings. The nanocomposite solutions suspended with s-CNFs show similar viscosity curves as compared to that of the u-CNFs filled system, Fig. 3(b). However, the shear thinning is observed to start at a lower filler loading of 0.5 wt%, which is due to the better dispersion of the s-CNFs after surface modification, as evidenced by the optical images shown in Fig. 4.

3.2.2 Effect of surface modification. Surface modification of the nanomaterials is widely used to improve the compatibility and interfacial interaction between nanofillers and polymer matrix.[55,56] Fig. 5 shows the effect of surface modification on the viscosity of CNFs suspended epoxy resin solutions. The viscosity is reported to increase with an increase of the particle loading as predicted by Mooney's Equation and MF theory.[57,58] More effective nanofillers are supposed to present in the unit solution within a more uniformly dispersed s-CNFs epoxy solution, which is supposed to have higher viscosity. However, the viscosity observed here is relatively lower in the nanocomposite solutions filled with s-CNFs than that observed in the nanocomposite solutions filled with u-CNFs. However, the difference in viscosity diminishes with the increase of shear rate owing to the orientation of the CNFs at high shear rate, especially in solutions with high particle loadings. The surface modification decreases the affinity and entanglement among CNFs, which lead to a better dispersion of s-CNFs in the epoxy resin, Fig. 4. The unusually lowered viscosity observed in s-CNF/epoxy solutions is different from the regular assumption that the suspension viscosity increases rapidly with an increase of the particle loading especially when the particles are in the nanometer range,[57–62] and is consistent with the recent observations in Fe_3O_4 nanoparticle suspended polyacronitrile dimethylformamide solution[4] and polyacrylonitrile dispersed 1-butyl-3-methylimidazolium chloride concentrated solutions.[63] The reduced viscosity after surface treatment is due to the better dispersion, which has also been observed in the fullerene and magnetite nanoparticles dispersed in polystyrene[64] and polystyrene nanoparticles in a linear polystyrene.[65] A similar phenomenon is observed in the $CaCO_3$ particles dispersed in a polyethylene matrix[66] and a poly(dimethyl siloxane) matrix,[67] in which agglomerated clusters increase the viscosity and surface treatment reduces the viscosity with an improved particle dispersion.[66,67]

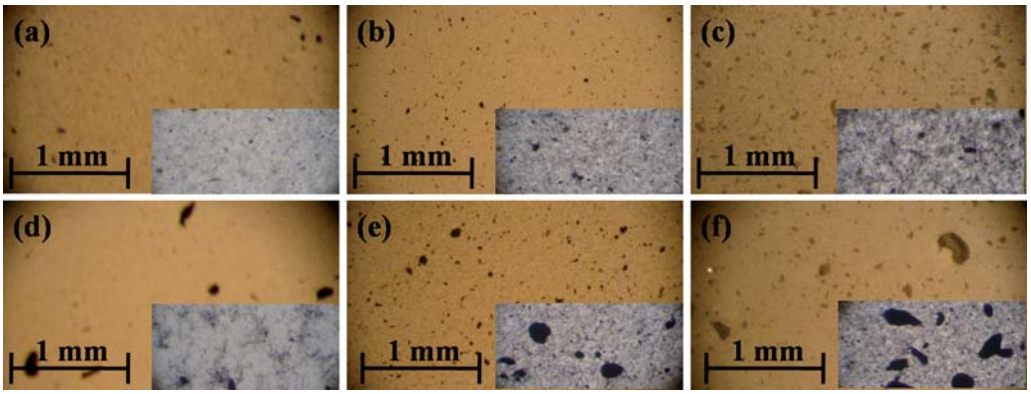

Fig. 4 Optical micrographs of epoxy resin suspension films filled with s-CNFs (a) 0.1 wt% (b) 0.3 wt% and (c) 0.5 wt%; and u-CNFs (d) 0.1 wt% (e) 0.3 wt% and (f) 0.5 wt%; insets are the images with larger magnification.

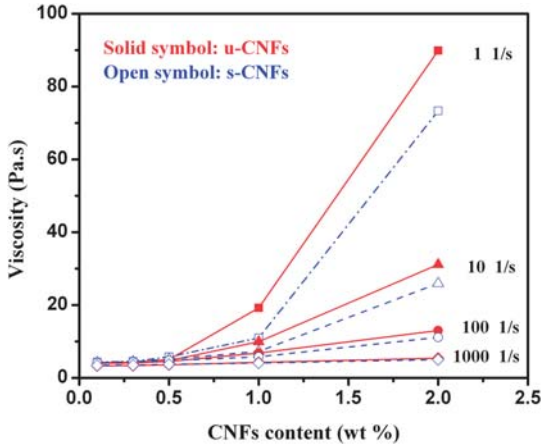

Fig. 5 Effect of surface modification on the viscosity of CNF/epoxy nanocomposite solutions suspended with different loadings under different shear rates at 25 °C.

3.2.3 Effect of temperature. The viscosity of melt polymers and solutions is strongly dependent on the testing temperature,[68,69] especially when some reactions occur during the heating process. The epoxy resin solutions suspended with either 1 wt% u-CNFs or 1 wt% s-CNFs are conducted at 25 °C, 50 °C, 75 °C and 120 °C, Fig. 6. It is well known that viscosity decreases with the increase of temperature due to the relaxation of polymer chains,[42,70,71] which is clearly shown in the curves from 25 °C to 50 °C, Fig. 6. The observed unusually lower viscosities for s-CNF filled solutions compared with those of the u-CNF filled solutions at each specific lower shear rate, Fig. 6, are due to the improved particle dispersion arising from the surface treatment, consistent with carbon nanotubes suspended epoxy resin solutions,[52,72] magnetic nanoparticles suspended polyurethane resin solutions[73] and a-zirconium phosphate (ZrP) nanoplatelets suspended epoxy monomers.[42] As the temperature increases to 75 °C, a small difference in viscosity is observed between the two epoxy resin solutions suspended with s-CNFs and u-CNFs. Interestingly, the viscosity of s-CNF/epoxy solution at 120 °C (curing temperature of epoxy) is significantly higher than that of

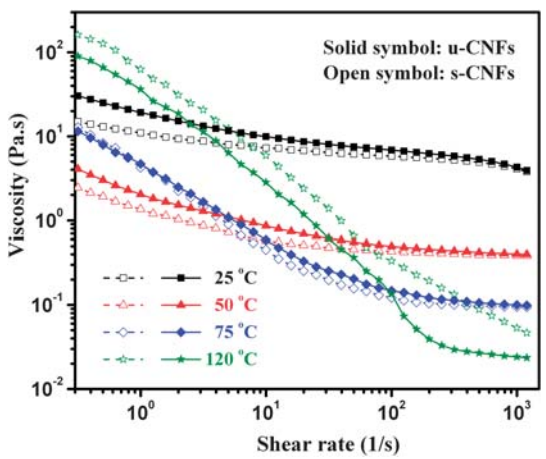

Fig. 6 Effect of temperature on the viscosity of epoxy resin solutions with a CNFs loading of 1 wt%.

the u-CNF/epoxy solution within the whole measured shear rate range. This distinctive transition of viscosity arises from the in situ reaction between the attached functional amine groups on the CNF surface and the epoxy monomer, the reaction mechanism is schematically described in Chart 2. Strong covalent bonding and interconnected network structure are formed after reaction, which makes the solution more resistant to external stresses and thus an increased viscosity was observed.

3.3 Thermal stability of cured epoxy nanocomposites

Fig. 7 shows the effect of CNF loading and surface modification on the thermal stability of the cured CNF/epoxy nanocomposites. All the samples are observed to have similar decomposition profiles and the degradation of the nanocomposites takes place in two stages. The first decomposition temperature (T_{d1}) is around 360 °C and the second decomposition temperature (T_{d2}) is around 550 °C. T_{d1} and T_{d2}, as well as the 5 wt% loss temperature ($T_{5\%}$), are summarized in Table 1. There is no report on which parts (bonds) decompose at the two different stages yet. However, there exists a relationship between bonding intensity and the decomposition, *i.e.*, a strong bond has a corresponding higher decomposition temperature, while a weak bond has a lower decomposition temperature.[74,75] Typical bond energies of C–C, C–O, C–N and C=C are 349, 370, 308, 614 kJ/mol, respectively.[76] The single bonds of C–C, C–O, C–N are susceptible to chain scission during thermal degradation and act as weak links, which correspond to the decomposition of epoxy at T_{d1}. The further decomposition at T_{d2} is attributed to the degradation of benzene rings, where the C–C bonding energy is between 614 kJ/mol (EC=C) and 698 kJ/mol (2EC–C).[75]

In the nanocomposites, the CNF loading does not appreciably affect the T_{d1} and T_{d2} of the nanocomposites reinforced with u-CNFs, the variation of T_{d1} and T_{d2} is less than 2.2 °C and 3.1 °C, respectively, as compared to those of the pristine epoxy. It is worth noticing that, except for the samples containing 0.1 wt% of u-CNFs, T_{d1} decreases slightly with the increase of CNF loading. This slight decrease of decomposition temperature is attributed to the increased free volume of nanocomposites upon the increased CNF loading, which is consistent with the results of PVAc/silicate nanocomposites.[77] Increased free volume fraction in polymer nanocomposites has been reported in polystyrene (PS) nanoparticle/linear PS composites[48] and fumed silica particles in glassy amorphous poly(4-methyl-2-pentyne).[65,78] The segmental motion is less constrained since the increased free volume provides larger free space between molecular chains. Thus, a lower decomposition temperature is observed. However, the decomposition temperatures of epoxy nanocomposites filled with 0.1 wt% and 0.3 wt% s-CNFs, Table 1, are slightly higher as compared to those of the nanocomposites filled with same amount of u-CNFs, and also higher than that of the pristine epoxy, which is due to an improved interfacial interaction (Fig. 11) resulting in a lower free volume.

The enhanced thermal stability of these PNCs is more obviously revealed in the second decomposition temperature (T_{d2}), which corresponds to the degradation of the polymer backbone.[79] Different from T_{d1}, T_{d2} is observed to be enhanced by 0.6–3.1 °C for the cured epoxy nanocomposites reinforced with different loadings of u-CNFs. This indicates that the

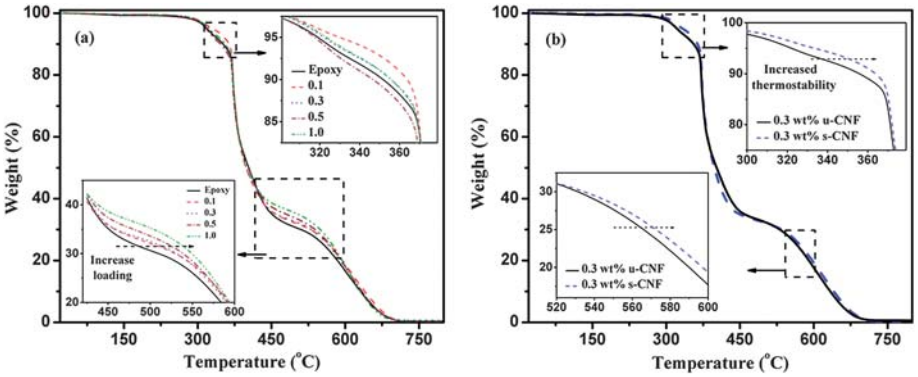

Fig. 7 TGA curves of (a) u-CNF/epoxy nanocomposites with different loadings and (b) nanocomposites filled with 0.3 wt% u-CNFs and s-CNFs.

cross-linking between epoxy monomers and curing agent is not affected by the addition of the u-CNFs, due to a complete wetting of the CNFs surface by the epoxy monomers as described in the Experimental. The thermal stability of the cured epoxy nanocomposites filled with s-CNFs is even better than those of both pristine epoxy and u-CNF/epoxy nanocomposites, as revealed by a higher T_{d2}, Table 1. Significant enhancements of T_{d2}, 7.5 °C and 5.2 °C, are observed in the epoxy nanocomposites reinforced even with a small amount (0.1 wt%) of s-CNFs as compared to those of the pristine epoxy and the nanocomposites filled with 0.1 wt% of u-CNFs. The increased stability is also clearly shown on the TGA curve of the cured epoxy PNCs filled with s-CNFs in both stages as compared to u-CNF/epoxy nanocomposites, Fig. 7(b). Both the improved dispersion of CNFs in the matrix and the covalent bonding contribute to the enhanced thermal stability. The initial thermal decomposition temperature ($T_{5\%}$) is defined as the temperature at which the total mass loss of 5% occurs. Compared to T_{d1} and T_{d2}, the enhancement of the initial degradation temperature for the cured epoxy nanocomposites filled with both u-CNFs and s-CNFs is more significant, Table 1. The $T_{5\%}$ increases by 14.4 °C and 11.4 °C for 0.3 wt% s-CNF/epoxy nanocomposites as compared to those of the pristine epoxy and 0.3 wt% u-CNF/epoxy nanocomposites, respectively.

3.4 Mechanical properties

3.4.1 DMA properties. Dynamic mechanical analysis (DMA) provides specific information on the storage modulus (G′), loss modulus (G″) and tanδ within the investigated temperature range. The storage modulus reflects the elastic modulus of nanocomposites while the loss modulus is related to the energy dissipation associated with the motion of polymer chains.[80] Fig. 8(a) shows the storage modulus as a function of the temperature for the pristine epoxy and its cured epoxy nanocomposites with various CNF loadings. G′ for the nanocomposites containing 0.1 wt% u-CNFs (3.17 GPa) is observed to be 166% larger than that of the cured pristine epoxy (1.19 GPa) within the glassy plateau (at 30 °C) and to be 176% larger within the rubbery plateau (at 200 °C) from 26.8 MPa to 9.72 MPa. The significant increase in G′ is due to the confinement and uniform dispersion of the CNFs in the matrix. However, only a slight change in G′ is observed for the cured epoxy nanocomposites filled with a u-CNF loading over 0.1 wt% as compared to that of the pristine cured epoxy, which is attributed to the agglomeration of CNFs (Fig. 4) and the weak interfacial bonding between CNFs and epoxy matrix (Fig. 10). A similar trend for G″ with the increase of temperature is observed, Fig. 8(b). The cured epoxy nanocomposites reinforced with 0.1 wt% u-CNFs have the highest G″ within the whole temperature range, which is increased by 141% and 189% as compared to those of the cured pristine epoxy within the glassy and rubbery plateaux, respectively. The increased G′ is ascribed to the constrained friction between polymer molecules after introducing CNFs in the polymer matrix.[81]

The tanδ is the ratio of the loss modulus to the storage modulus, and the peak of the tanδ is often used to determine the glass transition temperature (T_g). As seen in Fig. 8(c), the glass transition temperature (T_g) remains almost unchanged at about 119 °C upon incorporating various loadings of u-CNFs. This

Table 1 Tensile and thermal properties of CNF/epoxy nanocomposites

	Tensile properties			Thermal properties		
Composition	Tensile strength (MPa)	Young's modulus (GPa)	Elongation to break (%)	T_{d1} (°C)	T_{d2} (°C)	$T_{5\%}$ (°C)
Pristine Epoxy	72.3 ± 2.1	2.6 ± 0.1	4.3 ± 0.3	364.5	549.8	319.0
Epoxy/0.1 wt% u-CNFs	68.2 ± 1.3	2.6 ± 0.2	6.3 ± 0.1	364.8	552.1	328.0
Epoxy/0.3 wt% u-CNFs	76.5 ± 3.2	2.5 ± 0.3	6.7 ± 0.2	364.3	550.4	322.0
Epoxy/0.5 wt% u-CNFs	80.7 ± 1.0	2.9 ± 0.2	5.0 ± 0.3	362.3	550.4	320.4
Epoxy/1.0 wt% u-CNFs	76.9 ± 3.4	2.8 ± 0.3	4.5 ± 0.4	363.5	552.9	323.2
Epoxy/0.1 wt% s-CNFs	76.8 ± 2.7	2.2 ± 0.1	7.9 ± 0.3	365.0	557.3	330.3
Epoxy/0.3 wt% s-CNFs	81.3 ± 0.8	2.1 ± 0.2	6.8 ± 0.2	365.5	555.2	333.4

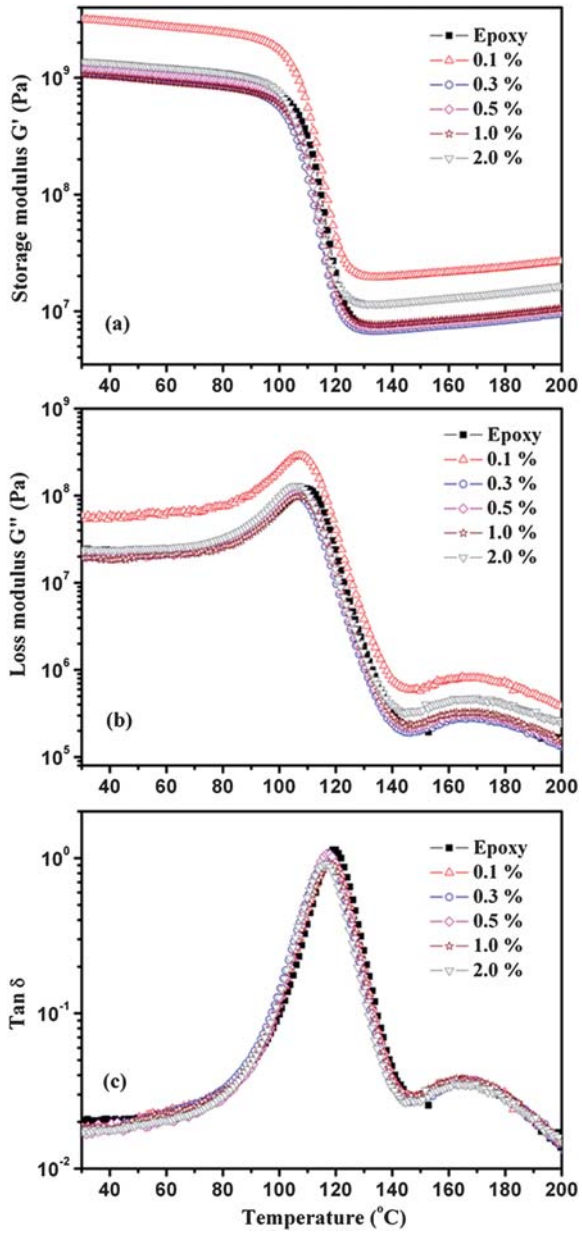

Fig. 8 (a) Storage modulus (G′), (b) loss modulus (G″) and (c) tanδ *vs.* temperature for the cured epoxy and its nanocomposites with different u-CNF loadings.

phenomenon is well consisted with the results reported in multiwalled carbon nanotubes reinforced nylon-6 nanocomposites.[81] In this case, the 1-d CNFs perform a similar role as the CNTs, and less strain is imposed on the polymer chain, thus the T_g of the nanocomposites is almost unchanged. Unlike the 2-d fillers, such as nanoclay platelets,[80] the polymer chain is greatly constrained between the nanolayers and usually increases the T_g of the cured epoxy nanocomposites.

Surface modification effect of CNFs on the DMA properties of the cured epoxy nanocomposites is also investigated in this work, Fig. 9. G′, G″ and tanδ are comparatively studied for the cured epoxy nanocomposites reinforced with both u-CNFs and s-CNFs at a filler loading of 0.3 wt% and 0.5 wt%, respectively. Both G′ and G″ are observed to significantly increase at around the glass transition temperature rather than at either low temperature (<80 °C) or high temperature (>150 °C), Fig. 9(a, b). Compared to that of the cured epoxy nanocomposites filled with u-CNFs, the sharp decrease of G′ upon the increase of temperature is delayed by 10 and 20 °C for the cured epoxy nanocomposites filled with 0.5 wt% and 0.3 wt% s-CNFs, respectively. The improvement of the thermal mechanical properties of epoxy nanocomposites filled with s-CNFs is attributed to the covalent bonding between s-CNFs and the epoxy monomers *via* the in situ reaction between amine-terminated functional groups on the wall of s-CNFs and epoxide groups. The covalent bonding thus restricts the mobility of the main chain of the epoxy resin by the

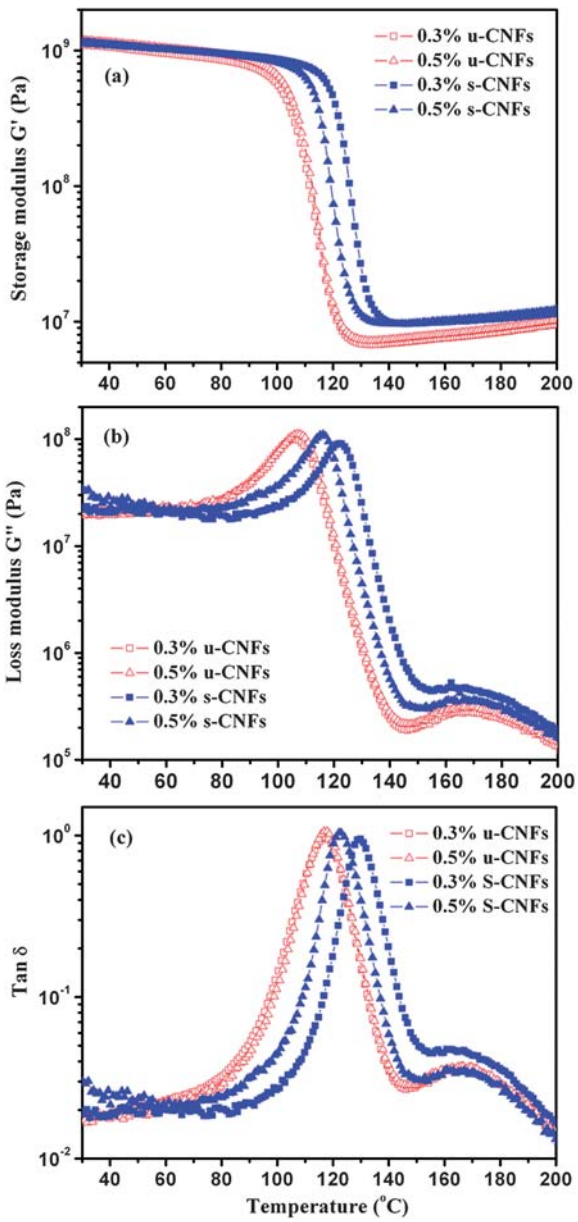

Fig. 9 (a) Storage modulus (G′), (b) loss modulus (G″) and (c) tanδ *vs.* temperature curves for nanocomposites with 0.3 wt% and 0.5 wt% u-CNFs and s-CNFs, respectively.

adhesive interfacial force between the filler and matrix. Therefore, the polymer undergoes higher temperature relaxation. Similar results are also observed in the G″, Fig. 9(b), which is about 10–20 °C enhancement for the cured epoxy nanocomposites filled with s-CNFs due to the increased adhesion between s-CNFs and the epoxy matrix.

Both an increase of storage modulus at high temperature, Fig. 8(a) and Fig. 9(a), and a second peak observed in the loss modulus, Fig. 8(b) and Fig. 9(b), have been used to study the curing extent.[82] Similar phenomena have been observed in silica particle (~5.5 μm) reinforced epoxy composites and explained in terms of curing conditions.[83] DSC is used to investigate the curing extent. The residue heat of the pure epoxy is measured to be 370 J/g. However, after the aforementioned curing process, the measured residue heat is negligible, 2.55 J/g (pure epoxy), 1.61 J/g (0.1 wt% u-CNFs), 0.22 J/g (0.3 wt% u-CNFs), 2.74 J/g (0.5 wt% u-CNFs), 2.84 J/g (0.1 wt% s-CNFs), 5.02 J/g (0.3 wt% s-CNFs) and 4.96 J/g (0.5 wt% s-CNFs), Fig. S1 (ESI†. The fraction of uncured epoxy in each sample is calculated to be 0.69% (pure epoxy), 0.44% (0.1 u-CNFs), 0.06% (0.3 u-CNFs), 0.74% (0.5 u-CNFs), 0.77% (0.1 s-CNFs), 1.4% (0.3 s-CNFs) and 1.3% (0.5 s-CNFs). The negligible uncured portion can not be fully responsible for the observed increase storage modulus at high temperature and the second peak in the loss modulus. This could be due to an inhomogeneous formation of epoxy networks.[82,84–86]

The peak of tanδ (T_g) shifts significantly to higher temperature for the cured epoxy nanocomposites filled with s-CNFs as compared to those of cured epoxy nanocomposites filled with u-CNFs, Fig. 9(c). This observation can be interpreted in the term of the interaction between s-CNFs and the epoxy matrix. It is well known that the T_g of a polymer depends on the mobility of the chain segment of the macromolecules in the polymer matrix. In the present case, the in situ reinforcement of CNFs on epoxy matrix restricts the motions of macromolecular chains and thus the glass transition temperatures of nanocomposites are increased.

3.4.2 Tensile properties. Fig. 10 shows the typical stress-strain curve of the cured epoxy nanocomposites as a function of CNF loading and the tensile properties are summarized in Table 1. The tensile strength increases as the u-CNFs loading increases up to 0.5 wt%, and experiences a slight decrease as the loading reaches 1wt%. This is due to the poor interaction between fibers and the polymer matrix (Fig. 11) and the agglomeration of u-CNFs owing to the high length-diameter (aspect) ratio and affinity. The highest tensile strength for the cured u-CNF/epoxy nanocomposites is 80.7 MPa at the loading of 0.5 wt%, which shows 11.5% increment as compared to that of the cured pristine epoxy (72.3 MPa). The tensile strength of the cured epoxy nanocomposites filled with s-CNF shows the favorable effects of the CNF surface treatment on the reinforcement of the epoxy resin. With the loadings of 0.1 wt% and 0.3 wt% of CNFs, the cured epoxy nanocomposites filled with s-CNFs show significant improvement in both tensile strength (12.6% and 6.3%) and elongation to break (25.4 and 1.5%) as compared to those of the cured epoxy nanocomposites filled with u-CNFs. The in situ reaction between the s-CNFs and epoxy matrix provides a strong covalent bonding, which not only promotes the compatibility

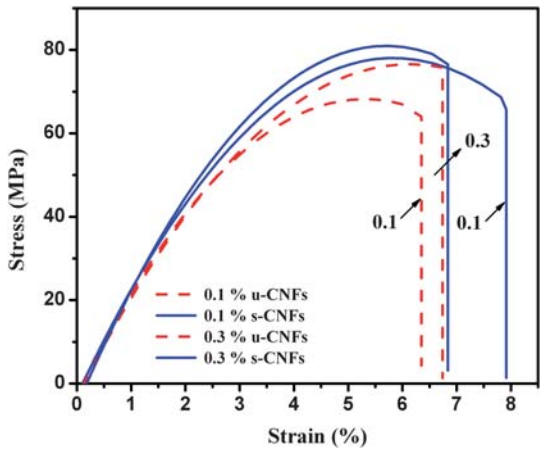

Fig. 10 Stress-strain curve of cured epoxy nanocomposites filled with different loadings of u-CNFs and s-CNFs.

between fibers and polymer but also increases the interfacial adhesion between these two phases. Therefore, the tensile strength increases in the cured epoxy nanocomposites. However, the Young's modulus of the s-CNF/epoxy nanocomposites is lower than that of the corresponding cured epoxy nanocomposites filled with u-CNFs, even lower than the pristine epoxy, Table 1. This indicates that the surface treated CNFs form an elastic interfacial layer between the CNFs and epoxy matrix, which is more sensitive to a large strain as reflected in the

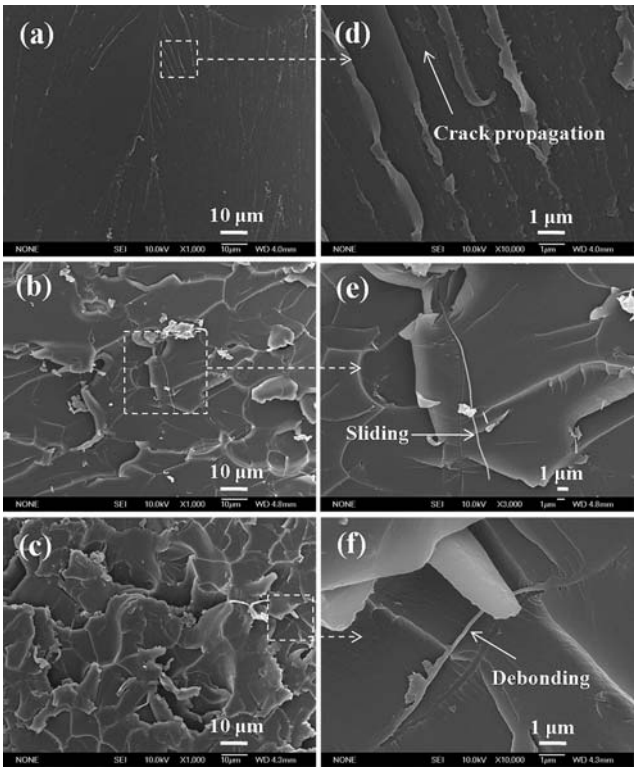

Fig. 11 SEM micrographs of (a) the cured pristine epoxy, and the nanocomposites filled with (b) 0.1 wt% u-CNFs and (c) 0.1 wt% s-CNFs; (d)–(f) show the enlarged fracture surfaces of (a)–(c), respectively.

increased elongation to break. The Young's modulus is calculated in the linear elastic region of the composites in the low strain region. Within this small strain, the stress is not high enough to break down the interfacial bonding, and the introduced "elastic layer" is easy to deform when a small stress is applied, thus a decreased Young's modulus is observed.

3.5 Microstructure of the fracture surface

Fig. 11 shows the SEM micrographs of fracture surfaces for cured pristine epoxy resin and nanocomposites filled with 0.1 wt% u-CNFs and s-CNFs. In micron scale, the cured neat epoxy shows a smooth fracture surface while the PNCs show a rough fracture surface, Fig. 11(a–c). The rough surface can be attributed to the matrix shear yielding or the polymer deformation between the CNFs, similar to the alumina nanoparticles reinforced vinyl ester resin nanocomposites.[30] Owning to the high mechanical strength and large aspect ratio of CNFs, it is considered to be one of the best materials to reinforce polymers with high load transfer efficiency. In this respect, the CNFs improve the toughness of the nanocomposites with the result that the matrix is amenable to a larger local plastic deformation. The enlarged SEM image of the cure pristine epoxy shows that the structural deformation is aligned in the same direction, Fig. 11(d). However, the cracking direction is interrupted by the addition of the CNFs, indicating that the stress is randomly distributed with the aid of CNFs. In addition, the mechanical properties of PNCs are strongly related to the interfacial properties between the matrix and fillers.[25,87] In this work, owning to the weak interfacial interaction between the epoxy matrix and u-CNFs, the u-CNFs are easily peeled off from the matrix, Fig. 11(e). However, strong interfacial interaction is observed in the case of the surface treated CNFs owning to the covalent bonding, Fig. 11(f). The strong interfacial interaction prevents the debonding of the fibers from the polymer matrix. Instead, the deformation is performed between the matrix and modifier layer on the CNF surface. Therefore, the local stress can be more efficiently transferred into the tougher CNFs, which results in a higher mechanical strength when the CNFs are in intimate contact with the epoxy matrix.

3.6 Electrical conductivity

Fig. 12 depicts the comparison of the volume resistivity of the cured epoxy nanocomposites filled with u-CNFs and s-CNFs. Generally, the resistivity is significantly higher for the cured epoxy nanocomposites filled with s-CNFs, an increased resistivity is also observed in polystyrene nanocomposites containing copper nanowires functionalized with 1-octanethiol.[88] However, the resistivity decreases slightly when the u-CNF loading is 0.1 wt%, Fig. 12. A further decrease of about eight orders of magnitude in the resistivity appears for u-CNF/epoxy nanocomposites with loadings varying from 0.1 wt% to 1 wt%. However, the resistivity does not change significantly when the loading is above 1 wt%, only a slight decrease of less than one order of magnitude is observed. This decrease in resistivity indicates an infinite network structure of percolated CNFs begins forming above 0.1 wt%. However, it is interesting to notice that the resistivity is above 10^{11} Ω cm when the loading increases to

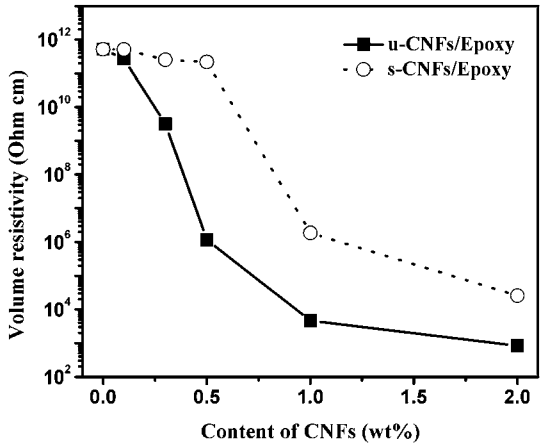

Fig. 12 Volume resistivities of the cured pure epoxy and cured epoxy nanocomposites filled with u-CNFs and s-CNFs.

0.5 wt% for s-CNF/epoxy nanocomposites. A sharp decrease in resistivity is observed from 0.5 wt% to 1 wt% for s-CNF/epoxy nanocomposites, but it is still two orders of magnitude larger as compared to u-CNF/epoxy nanocomposites at the loading of 1 wt%.

The effect of oxidation on the electrical conductivity of CNTs is still controversial. Kim *et al.* reported that the crystalline structure of multiwalled carbon nanotubes (MWNTs) is partially damaged after oxidation, which leads to the reduction of electrical conductivity of chemically modified MWNT/epoxy composites.[89] However, Li *et al.* reported an increased conductivity of CNT fibers after oxidation and suggested that the enhanced conductivity is arising from the induced defects on the CNT surface.[90] In this work, a further step of modification is introduced through the reaction between silane and oxidized CNFs, and the decreased conductivity is observed as compared to that of the as-received CNFs, Fig. 12. This indicates that an organo-layer is formed on CNF surface after silanization, which serves as an insulating layer and partially blocks the effective electron transportation among CNFs, the schematic mechanism of electron transfer behavior between CNFs before and after surface modification is presented in Fig. 13. Fewer electrons are able to cross the organo-layer and thus a higher resistivity is observed.

4. Conclusions

Dynamic rheological measurements of epoxy resin nanocomposite suspensions filled with different loadings of u-CNFs

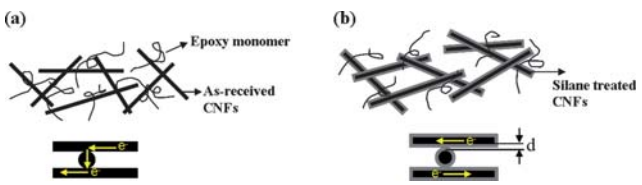

Fig. 13 Contact model of CNFs in epoxy solutions suspended with (a) as-received CNFs and (b) silane treated CNFs.

and s-CNFs are performed at different shear rates. Results have demonstrated that the suspensions exhibit a transition from Newtonian behavior to shear thinning behavior with the increase of the CNF loadings, and shear thinning behavior is observed at a lower loading for s-CNFs. The change of complex viscosity at different temperatures (25, 50, 75 and 120 °C) reveals that the interfacial reaction is strongly temperature dependent and is accelerated at higher temperatures. The resulting tensile properties of both the u-CNF/epoxy and s-CNF/epoxy nanocomposites indicate a more efficient load transfer between the s-CNFs and epoxy matrix. The tensile strength and elongation-to-break of 0.1 wt% s-CNF/epoxy nanocomposites are 12.6% and 25.4% higher than those of the 0.1 wt% u-CNF/epoxy nanocomposites. Dynamic mechanical properties show that the CNF loading does not affect the glass transition temperature. However, with surface modification, the glass transition temperature shifted to higher temperature by 10–20 °C owing to the introduced interfacial interaction. TGA analysis further indicates a better thermal stability for the s-CNF/epoxy nanocomposites. The interfacial interaction between s-CNFs and epoxy matrix is clearly presented by SEM images and the rough surface morphology of nanocomposites represents the effective load transfer of the CNFs within the matrix. The electrical resistance decreases by 7 orders of magnitude with the addition of 1 wt% u-CNFs. However, the resistivity is a hundred times higher with the same loading after modification of the CNFs surface due to the introduced insulating layer.

Acknowledgements

This work is supported by a research start-up fund from Lamar University. Partial financial support from Northrop Grumman Corporation is kindly acknowledged. The financial support from Dan F. Smith Department of Chemical Engineering and College of Engineering at Lamar University for obtaining the TA rheometer is kindly acknowledged.

References

1 K.-t. Lau, M. Lu, L. Chun-ki, H.-y. Cheung, F.-L. Sheng and H.-L. Li, *Compos. Sci. Technol.*, 2005, **65**, 719–725.
2 J. Cho, J. Y. Chen and I. M. Daniel, *Scr. Mater.*, 2007, **56**, 685–688.
3 X.-L. Xie, Q.-X. Liu, R. K.-Y. Li, X.-P. Zhou, Q.-X. Zhang, Z.-Z. Yu and Y.-W. Mai, *Polymer*, 2004, **45**, 6665–6673.
4 D. Zhang, A. B. Karki, D. Rutman, D. P. Young, A. Wang, D. Cocke, T. H. Ho and Z. Guo, *Polymer*, 2009, **50**, 4189–4198.
5 Z. Guo, T. Y. Kim, K. Lei, T. Pereira, J. G. Sugar and H. T. Hahn, *Compos. Sci. Technol.*, 2008, **68**, 164–170.
6 Z. Guo, S. Park, S. Wei, T. Pereira, M. Moldovan, A. B. Karki, D. P. Young and H. T. Hahn, *Nanotechnology*, 2007, **18**, 335704.
7 D. Zhang, R. Chung, A. B. Karki, F. Li, D. P. Young and Z. Guo, *J. Phys. Chem. C*, 2010, **114**, 212–219.
8 V. L. Pushparaj, M. M. Shaijumon, A. Kumar, S. Murugesan, L. Ci, R. Vajtai, R. J. Linhardt, O. Nalamasu and P. M. Ajayan, *Proc. Natl. Acad. Sci. U. S. A.*, 2007, **104**, 13574–13577.
9 P. Kim, N. M. Doss, J. P. Tillotson, P. J. Hotchkiss, M.-J. Pan, S. R. Marder, J. Li, J. P. Calame and J. W. Perry, *ACS Nano*, 2009, **3**, 2581–2592.
10 P. Vacca, G. Nenna, R. Miscioscia, D. Palumbo, C. Minarini and D. D. Sala, *J. Phys. Chem. C*, 2009, **113**, 5777–5783.
11 A. F. Nogueira, B. S. Lomba, M. A. Soto-Oviedo, C. R. D. Correia, P. Corio, C. A. Furtado and I. A. Hummelgen, *J. Phys. Chem. C*, 2007, **111**, 18431–18438.
12 Z. Guo, S. Park, H. T. Hahn, S. Wei, M. Moldovan, A. B. Karki and D. P. Young, *J. Appl. Phys.*, 2007, **101**, 09M511.
13 T. Shimada, K. Ookubo, N. Komuro, T. Shimizu and N. Uehara, *Langmuir*, 2007, **23**, 11225–11232.
14 Z. Wen, S. Ci and J. Li, *J. Phys. Chem. C*, 2009, **113**, 13482–13487.
15 Z. Guo, H. T. Hahn, H. Lin, A. B. Karki and D. P. Young, *J. Appl. Phys.*, 2008, **104**, 014314.
16 Z. Guo, S. Park, H. T. Hahn, S. Wei, M. Moldovan, A. B. Karki and D. P. Young, *Appl. Phys. Lett.*, 2007, **90**, 053111.
17 D. S. Koktysh, X. Liang, B. G. Yun, I. Pastoriza-Santos, R. L. Matts, M. Giersig, C. Serra-Rodríuez, L. M. Liz-Marzán and N. A. Kotov, *Adv. Funct. Mater.*, 2002, **12**, 255.
18 S. Liu, L. Wei, L. Hao, N. Fang, M. W. Chang, R. Xu, Y. Yang and Y. Chen, *ACS Nano*, 2009, **3**, 3891–3902.
19 K.-T. Hsiao, J. Alms and S. G. Advani, *Nanotechnology*, 2003, **14**, 791–793.
20 T. H. Ho and C.-S. Wang, *J. Appl. Polym. Sci.*, 1994, **54**, 13–23.
21 P. M. Hergenrother, C. M. Thompson, J. J. G. Smith, J. W. Connell, J. A. Hinkley, R. E. Lyon and R. Moulton, *Polymer*, 2005, **46**, 5012–5024.
22 W. Zheng and S.-C. Wong, *Compos. Sci. Technol.*, 2003, **63**, 225–235.
23 J. K. W. Sandler, J. E. Kirk, I. A. Kinloch, M. S. P. Shaffer and A. H. Windle, *Polymer*, 2003, **44**, 5893–5899.
24 H. G. Yoon, K. W. Kwon, K. Nagata and K. Takahashi, *Carbon*, 2004, **42**, 1877–1879.
25 S. Kang, S. I. Hong, C. R. Choe, M. Park, S. Rim and J. Kim, *Polymer*, 2001, **42**, 879.
26 M. Zanetti, G. Camino, D. Canavese, A. B. Morgan, F. J. Lamelas and C. A. Wilkie, *Chem. Mater.*, 2002, **14**, 189–193.
27 J. Zhu, A. B. Morgan, F. J. Lamelas and C. A. Wilkie, *Chem. Mater.*, 2001, **13**, 3774.
28 G. M. Whitesides, J. P. Mathias and C. T. Seto, *Science*, 1991, **254**, 1312–1319.
29 T. Lan, P. D. Kaviratna and T. J. Pinnavaia, *Chem. Mater.*, 1995, **7**, 2144–2150.
30 Z. Guo, T. Pereira, O. Choi, Y. Wang and H. T. Hahn, *J. Mater. Chem.*, 2006, **16**, 2800.
31 J. Liu, Z. Yue and H. Fong, *Small*, 2009, **5**, 536–542.
32 D. Tasis, N. Tagmatarchis, A. Bianco and M. Prato, *Chem. Rev.*, 2006, **106**, 1105–1136.
33 H.-X. Wu, R. Tong, X.-Q. Qiu, H.-F. Yang, Y.-H. Lin, R.-F. Cai and S.-X. Qian, *Carbon*, 2007, **45**, 152–159.
34 S. Banerjee, T. Hemraj-Benny and S. S. Wong, *Adv. Mater.*, 2005, **17**, 17–29.
35 Y. Yang, X. Xie, Z. Yang, X. Wang, W. Cui, J. Yang and Y.-W. Mai, *Macromolecules*, 2007, **40**, 5858–5867.
36 C. A. Mitchell and R. Krishnamoorti, *Macromolecules*, 2007, **40**, 1538–1545.
37 W. Chen, H. Lu and S. R. Nutt, *Compos. Sci. Technol.*, 2008, **68**, 2535–2542.
38 W. Chen, M. L. Auad, R. J. J. Williams and S. R. Nutt, *Eur. Polym. J.*, 2006, **42**, 2765.
39 Y. Y. Huang, S. V. Ahir and E. M. Terentjev, *Phys. Rev. B: Condens. Matter Mater. Phys.*, 2006, **73**, 125422.
40 Q. Zhang, F. Fang, X. Zhao, Y. Li, M. Zhu and D. Chen, *J. Phys. Chem. B*, 2008, **112**, 12606–12611.
41 L. Le Pluart, J. Duchet, H. Sautereau, P. Halley and J. F. Gerard, *Appl. Clay Sci.*, 2004, **25**, 207–219.
42 L. Sun, W.-J. Boo, J. Liu, A. Clearfield, H.-J. Sue, N. E. Verghese, H. Q. Pham and J. Bicerano, *Macromol. Mater. Eng.*, 2009, **294**, 103–113.
43 J. Wang, Z. Fang, A. Gu, L. Xu and F. Liu, *J. Appl. Polym. Sci.*, 2006, **100**, 97–104.
44 A. S. M. Chong and X. S. Zhao, *J. Phys. Chem. B*, 2003, **107**, 12650–12657.
45 Y.-Y. Song, H. Hildebrand and P. Schmuki, *Surf. Sci.*, 604, 346–353.
46 H. J. Martin, K. H. Schulz, J. D. Bumgardner and K. B. Walters, *Appl. Surf. Sci.*, 2008, **254**, 4599–4605.
47 W. Wu, Q. He, H. Chen, J. Tang and L. Nie, *Nanotechnology*, 2007, **18**, 145609.
48 J. Kathi and K. Rhee, *J. Mater. Sci.*, 2008, **43**, 33–37.
49 K. M. R. Kallury, U. J. Krull and M. Thompson, *Anal. Chem.*, 1988, **60**, 169–172.
50 D. C. Erickson, D. Li, T. M. White and J. Gao, *Ind. Eng. Chem. Res.*, 2001, **40**, 3523.
51 J. L. Duda, E. E. Klaus and S. C. Lin, *Ind. Eng. Chem. Res.*, 1988, **27**, 352–361.

52 S. S. Rahatekar, K. K. K. Koziol, S. A. Butler, J. A. Elliott, M. S. P. Shaffer, M. R. Mackley and A. H. Windle, *J. Rheol.*, 2006, **50**, 599–610.
53 Y. H. Hyun, S. T. Lim, H. J. Choi and M. S. Jhon, *Macromolecules*, 2001, **34**, 8084–8093.
54 R. Krishnamoorti, R. A. Vaia and E. P. Giannelis, *Chem. Mater.*, 1996, **8**, 1728–1734.
55 C.-H. Tseng, C.-C. Wang and C.-Y. Chen, *Chem. Mater.*, 2007, **19**, 308–315.
56 H.-L. Tyan, C.-M. Leu and K.-H. Wei, *Chem. Mater.*, 2001, **13**, 222–226.
57 D. W. Sundstrom, *Rheol. Acta*, 1983, **22**, 420–423.
58 H. Choi, C. Kim, T. M. Kwon and M. S. Jhon, *J. Magn. Magn. Mater.*, 2000, **209**, 228.
59 P. Pötschke, T. D. Fornes and D. R. Paul, *Polymer*, 2002, **43**, 3247–3255.
60 L. Jiang, Y. C. Lam, K. C. Tam, T. H. Chua, G. W. Sim and L. S. Ang, *Polymer*, 2005, **46**, 243–252.
61 D. Ratna and G. P. Simon, *Polymer*, 2001, **42**, 8833–8839.
62 V. Yong and H. T. Hahn, *J. Appl. Polym. Sci.*, 2006, **102**, 4365–4371.
63 W. Liu, L. Cheng, H. Zhang, Y. Zhang, H. Wang and M. Yu, *Int. J. Mol. Sci.*, 2007, **8**, 180–188.
64 A. Tuteja, P. M. Duxbury and M. E. Mackay, *Macromolecules*, 2007, **40**, 9427–9434.
65 M. E. Mackay, T. T. Dao, A. Tuteja, D. L. Ho, B. V. Horn, H.-C. Kim and C. J. Hawker, *Nat. Mater.*, 2003, **2**, 762–766.
66 M. A. Osman and A. Atallah, *Polymer*, 2005, **46**, 9476–9488.
67 T. Kaully, A. Siegmann and D. Shacham, *Polym. Adv. Technol.*, 2007, **18**, 696–704.
68 R. Wagener and T. J. G. Reisinger, *Polymer*, 2003, **44**, 7513–7518.
69 B. Yoo, *J. Texture Stud.*, 2003, **34**, 53–67.
70 T. G. Fox and P. J. Flory, *J. Am. Chem. Soc.*, 1948, **70**, 2384–2395.
71 G. M. Barrow, *Physical Chemistry*, McGraw-Hill, New York, 1996.
72 J. Qiu, C. Zhang, B. Wang and R. Liang, *Comput. Mater. Sci.*, 2009, **44**, 1379–1385.
73 C.-N. Shauo and C.-G. Chao, *Jpn. J. Appl. Phys.*, 2006, **45**, 5746–5753.
74 H. Zhao, J. Gao, Y. Li and S. Shen, *J. Therm. Anal. Calorim.*, 2003, **74**, 227–236.
75 M. Kinoshita, T. Nemoto, T. Souda and K. Takeda, *Polym. Degrad. Stab.*, 2000, **68**, 437.
76 G. Montaudo, C. Puglisi, E. Scamporrino and D. Vitalini, *Macromolecules*, 1984, **17**, 1605–1614.
77 Y. Shi, S. Peterson and D. Y. Sogah, *Chem. Mater.*, 2007, **19**, 1552–1564.
78 T. C. Merkel, B. D. Freeman, R. J. Spontak, Z. He, I. Pinnau, P. Meakin and A. J. Hill, *Science*, 2002, **296**, 519–522.
79 H. Liu, S. Zheng and K. Nie, *Macromolecules*, 2005, **38**, 5088–5097.
80 H.-B. Hsueh and C.-Y. Chen, *Polymer*, 2003, **44**, 5275–5283.
81 T. Liu, I. Y. Phang, L. Shen, S.-Y. Chow and W.-D. Zhang, *Macromolecules*, 2004, **37**, 7214–7222.
82 J. Mijovic and K.-F. Lin, *J. Appl. Polym. Sci.*, 1986, **32**, 3211–3227.
83 T. Adachi, W. Araki, T. Nakahara, A. Yamaji and M. Gamou, *J. Appl. Polym. Sci.*, 2002, **86**, 2261–2265.
84 J. Duchet and J. P. Pascault, *J. Polym. Sci., Part B: Polym. Phys.*, 2003, **41**, 2422–2432.
85 K. Duscaronek, *Angew. Makromol. Chem.*, 1996, **240**, 1–15.
86 H. Kishi, T. Naitou, S. Matsuda, A. Murakami, Y. Muraji and Y. Nakagawa, *J. Polym. Sci., Part B: Polym. Phys.*, 2007, **45**, 1425–1434.
87 A. Eitan, K. Jiang, D. Dukes, R. Andrews and L. S. Schadler, *Chem. Mater.*, 2003, **15**, 3198–3201.
88 G. A. Gelves, B. Lin, U. Sundararaj and J. A. Haber, *Nanotechnology*, 2008, **19**, 215712.
89 Y. J. Kim, T. S. Shin, H. D. Choi, J. H. Kwon, Y.-C. Chung and H. G. Yoon, *Carbon*, 2005, **43**, 23–30.
90 Q. Li, Y. Li, X. Zhang, S. B. Chikkannanavar, Y. Zhao, A. M. Dangelewicz, L. Zheng, S. D. Doorn, Q. Jia, D. E. Peterson, P. N. Arendt and Y. Zhu, *Adv. Mater.*, 2007, **19**, 3358.

